Journal of Alloys and Compounds 504 (2010) 102–109

Contents lists available at ScienceDirect

Journal of Alloys and Compounds

journal homepage: www.elsevier.com/locate/jallcom

Mechanical alloying of Cu–*x*Cr (*x* = 3, 5 and 8 wt.%) alloys

C. Aguilar[a,*], S. Ordoñez[b], D. Guzman[c], P.A. Rojas[d]

[a] Instituto de Materiales y Procesos Termomecánicos, Facultad de Ciencias de la Ingeniería, Universidad Austral de Chile, General Lagos 2086, Valdivia, Chile
[b] Departamento de Ingeniería Metalúrgica, Facultad de Ingeniería, Universidad de Santiago de Chile, Av. L. Bernardo O'Higgins 3363, Santiago, Chile
[c] Departamento de Metalurgia, Facultad de Ingeniería, Universidad de Atacama, Av. Copayapu 485, Copiapó, Chile
[d] Escuela de Ingeniería Mecánica, Facultad de Ingeniería, Pontificia Universidad Católica de Valparaíso, Av. Los Carrera 01567, Quilpué, Chile

ARTICLE INFO

Article history:
Received 1 September 2009
Received in revised form 10 May 2010
Accepted 14 May 2010
Available online 27 May 2010

Keywords:
Mechanical alloying
Copper alloys
Nanostructure
XRD
SEM

ABSTRACT

This work studies the structural evolution of Cu–*x*Cr (*x* = 3, 5 and 8 wt.%) alloys processed by mechanical alloying using X-ray diffraction profiles, scanning microscopy and microhardness analysis. X-ray diffraction analysis using the modified Williamson–Hall and Warren–Averbach methods were used to determine structural properties, such as crystallite size, stacking fault probability and energy, dislocation density, lattice parameters and crystallite size distribution of metallic powder as a function of Cr amount and milling time. Lattice defects increase the Gibbs free energy and the Gibbs free energy curves shift upward, therefore the solubility limit change.

1. Introduction

It is interesting to pursue the development of novel high performance materials due to modern-day demand. For this reason, nanomaterials are very interesting because they exhibit an unusual combination of properties such as strength, good ductility, high fracture toughness, and good corrosion resistance [1]. These new and unsuspected chemical and physical properties are not found in coarse-grained materials [2]. Recently, the synthesis of amorphous, intermetallic, and nanocrystalline materials has received attention. These materials can be obtained by non-equilibrium processes, such as mechanical alloying (MA), rapid solidification, vapor phase condensation, or irradiation/ion implantation. MA is a simple and versatile process that transfers high amounts of energy from milling balls to the alloy powder during the milling process [3]. MA is a dry, solid-state powder processing technique involving repeated welding, fracturing and re-welding of powder particles in a high-energy ball mill [3]. The main attributes of MA are the extension of a solid solution, refinement of structures in the nanometer range, production of fine dispersion of a second phase, and synthesis of novel crystalline, quasi-crystalline and amorphous phases. The main objective of this work is to analyze the synthesis of Cu–*x*Cr alloys (*x* = 3, 5 and 8 wt.%) by MA and to study the solid solution extension of Cr into Cu. The Cu–Cr system exhibits a very limited equilibrium mutual solubility (0.8 at.% Cr in fcc-Cu) at the eutectic melting temperature of 1075 °C [4], whereas the solubility of Cu in bcc-Cr is negligible.

2. Experimental procedure

The experiments were performed using copper and chromium powders. The copper was 99 wt.% Cu, contained less than 1000 ppm of oxygen and particle sizes ranged between 170 and 400 mesh. The chromium powder particle sizes ranged between 170 and 325 mesh. In a typical run, copper powder was mixed with chromium (3, 5 and 8 wt.%), and the mixture was placed in a 25 ml stainless steel container and milled in a SPEX 8000D mill with argon for 0.5, 4, 8 and 50 h. Stainless steel balls of 8 mm diameter using a constant balls/powder ratio of 10:1. The X-ray diffraction (XRD) analysis was conducted in a Siemens D5000 diffractometer with copper radiation of $K\alpha_1$ = 0.154056 nm, and annealing pure copper was used the standard. Whole patterns were measured in an angular range between 38° and 120° in 2θ and a Jeol 5410 was used for scanning electron microscopy (SEM).

3. Results and discussion

3.1. XRD results

X-ray diffraction analysis was used to obtain structural features of the Cu–Cr alloys. X-ray patterns shows typical behavior of mechanically alloyed metallic powders [3], increase of peak broadening, shift of diffraction lines, disappearance of lines of diffractions of solute due to severe plastic deformation, as shown in Fig. 1. As a reference, the X-ray pattern of pure un-milled Cu is shown. The strongest Cr peak is {1 1 0}, which is around $2\theta = 44.39°$ [5], and it disappears at milling times of 0.5, 8 and 50 h for 3, 5 and 8 wt.%Cr

* Corresponding author. Tel.: +56 63 221863; fax: +56 63 221033.
E-mail address: ceaguilar@uach.cl (C. Aguilar).

0925-8388/$ – see front matter © 2010 Elsevier B.V. All rights reserved.
doi:10.1016/j.jallcom.2010.05.061

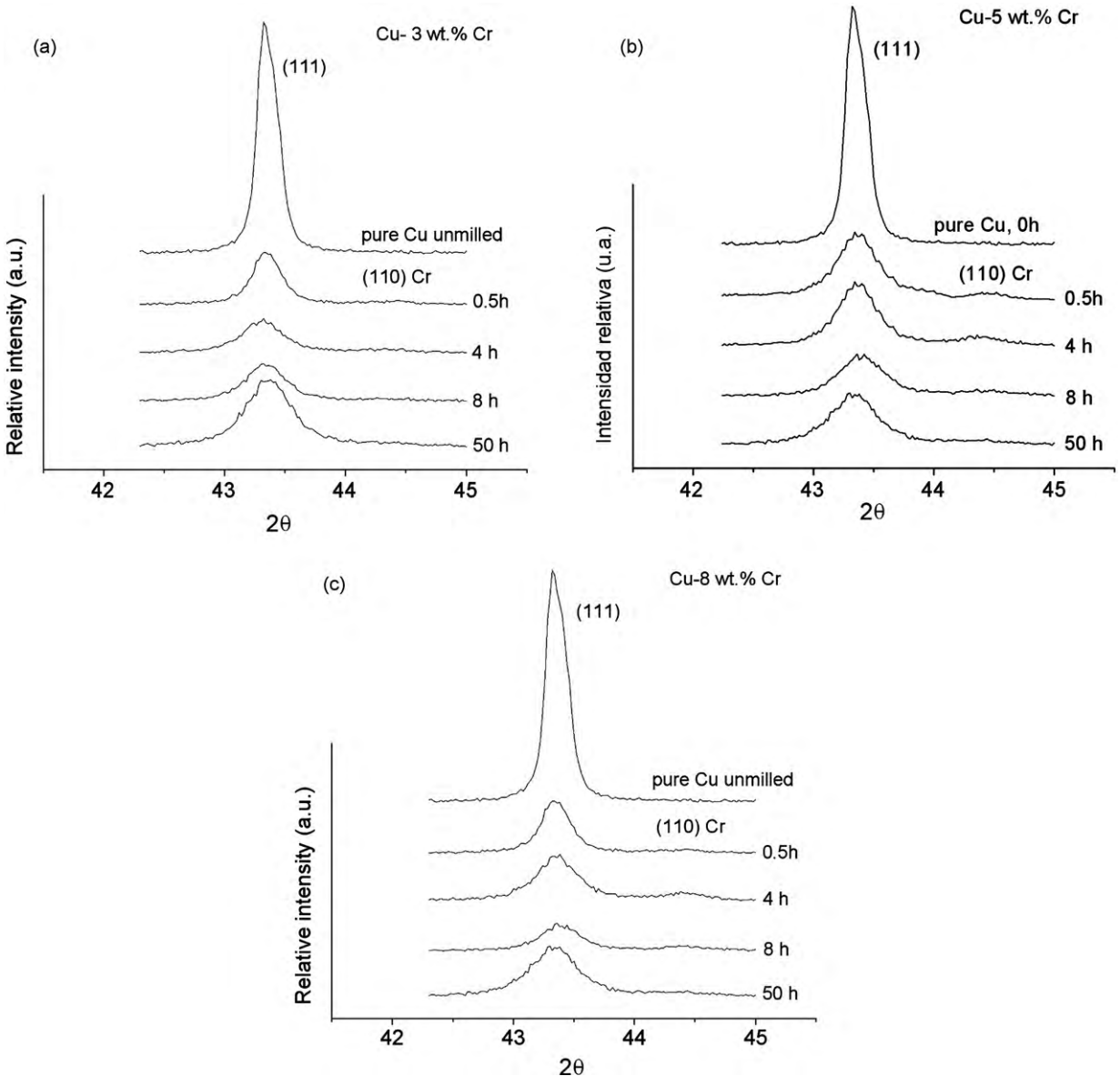

Fig. 1. X-ray diffraction patterns of (a) Cu–3%Cr, (b) Cu–5%Cr and (c) Cu–8%Cr.

alloys, respectively. The disappearance of this peak is frequently assumed to be the formation of solid solution [3].

X-ray diffraction peak analysis was made applying the modified Warren–Averbach method, Eq. (1) [6], where A(L) is real Fourier coefficient, d is the area averaged crystallite size (or grain size), $L = na_3$ is a distance normal to the reflecting planes $\{h\,k\,l\}$, n is the harmonic number, $a_3 = \lambda/2(\sin\theta_2 - \sin\theta_1)$, and $(\theta_2 - \theta_1)$ is the angular range of the measured diffraction profile, θ is the Bragg angle, λ is the X-ray wavelength, ρ is the dislocation density, $B = \pi b^2/2$, b is the Burger vector, Re is the effective outer cutoff radius of dislocations, R_1 and R_2 are the auxiliary parameters and $\bar{C}$ are the average contrast factors. This method considers anisotropic strain using a dislocation model based on the mean square strain of dislocated crystals [7,8]. This model uses dislocation contrast factors (C) to take into account the contribution of a dislocation strain on diffraction profile broadening, which depends on the relative orientations of the line (l) and Burger vector (b) of the dislocation and diffraction vector (g). Thus average contrast factors can be expresses as $\bar{C} = \bar{C}_{h00}(1 - qH^2)$ [9], where q is a constant, $\bar{C}_{h00}$ is the average dislocation contrast factor for the $h\,0\,0$ reflections, $H^2 = (h^2k^2 + k^2l^2 + l^2h^2)/(h^2 + k^2 + l^2)^2$, and $h\,k\,l$ are Miller indices.

$$\ln\ A(L) \cong -\left(\frac{L}{d}\right) - \rho BL^2 \ln\left(\frac{R_e}{L}\right)(K^2\bar{C}) + QB^2L^4 \ln\left(\frac{R_1}{L}\right)\ln\left(\frac{R_2}{L}\right)(K^2\bar{C})^2 \quad (1)$$

3.1.1. Determination of average contrast factors $\bar{C}$

3.1.1.1. Determination of q. From the linear regression of the left hand side versus H^2 of Eq. (2) the parameter q can be determined experimentally [9] where $\Delta K = 2\cos\theta(\Delta\theta)/\lambda$, $K = 2\sin\theta/\lambda$ [10], $\phi = (c/D)^2$, $\beta = \pi A^2 b^2 \rho/2$ and A one parameter determined by Re.

$$\left(\frac{\Delta K^2 - \phi}{K^2}\right) = \beta\bar{C}_{h\,00}(1 - qH^2) \quad (2)$$

Table 1 lists q values calculated with Eq. (2). The theoretically calculated pure edge and screw dislocation q parameters for pure

Table 1
q values of the Cu–Cr alloys.

% Cr	Milling time (h)			
	0.5	4	8	50
3	1.83	2.23	1.63	1.65
5	1.86	2.13	1.74	1.90
8	2.03	1.41	2.31	2.35

Cu are $q_{edge} = 1.63$ and $q_{screw} = 2.37$ [9] for the system $\{1\,1\,1\}\langle 1\,1\,0\rangle$. Due to the low percentage of Cr used in this study theses values were assumed for the Cu–Cr alloys. Observing theses values, Table 1, all experimental q values of the Cu–Cr alloys are inside this range. However if an experimental q value were out of this range, a different dislocation type that provides a larger q value range could be considered, such as the $\langle 1\,1\,1\rangle\{1\,1\,0\}$ type dislocations in fcc crystals, which are prismatic loops as observed by TEM [11].

3.1.1.2. Determination of $\bar{C}_{h00}$. The $\bar{C}_{h00}$ values can be determined from Fig. 2 [9], where $\bar{C}_{h00}$ is shown as a function of A and c_{12}/c_{44} for pure edge and screw dislocations (A is the Zener factor and c_{ij} are elastic coefficients). Due to the low percentage of Cr used in this study, the c_{ij} of all alloys were approximated by pure Cu. The c_{ij} values are: $c_{11} = 168.4$ GPa, $c_{12} = 121.4$ GPa and $c_{44} = 75.4$ GPa [12]. Therefore, the Zener factor and c_{12}/c_{44} ratio are 3.208 and 1.61, respectively. The value found was $\bar{C}_{h00} = 0.3040$, which it will be used for all Cu–Cr alloys. Finally with $\bar{C}_{h00}$ and q, the average contrast factors, $\bar{C}$, can be determined as a function of milling time and percentage of Cr using $\bar{C} = \bar{C}_{h00}(1 - qH^2)$ [9].

Fig. 3 shows a comparison of results obtained by modified Williamson–Hall method (MWH) [6] and traditional

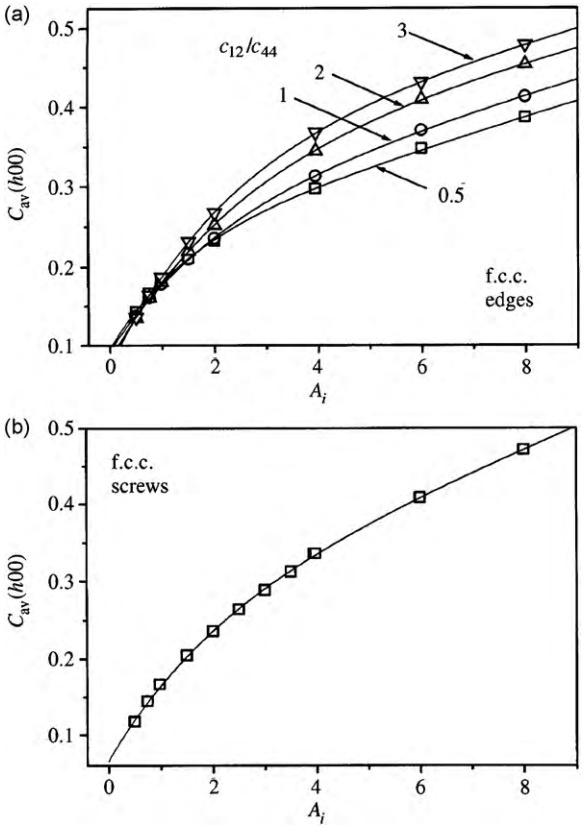

Fig. 2. The average contrast factors of the $h\,0\,0$ reflections for fcc crystals: (a) edge and (b) screw [9].

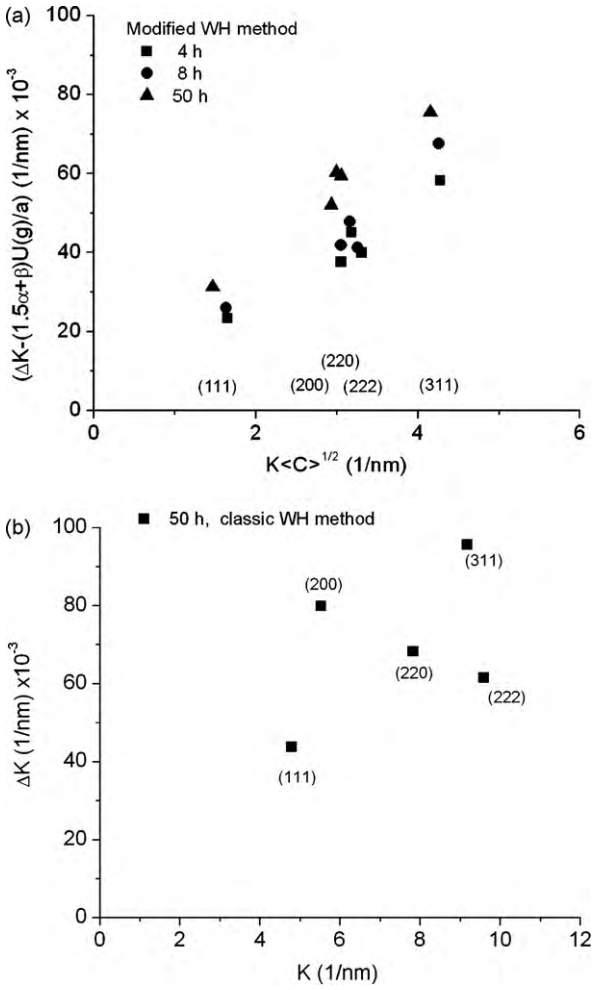

Fig. 3. Example of plots of the modified Williamson–Hall method for a Cu–5%Cr alloy at (a) 4, 8 and 50 h, and (b) plot of the traditional Williamson–Hall method for a Cu–5%Cr alloy at 50 h.

Williamson–Hall method (WH) [13] for a Cu–5%Cr alloy, respectively. The MWH take account anisotropic strain and WH isotropic strain. Fig. 3(a) shows that when increase milling time increases, ΔK shifts upward, indicating a decrease of crystallite size and increase in dislocation density (Fig. 4(a) and (b), respectively). Similar behavior for all Cu–Cr alloys was found. Fig. 3(b) shows an example of the traditional Williamson–Hall method [13], for the Cu–5%Cr alloy milled for 50 h. It is possible to observe that the ΔK values of the $\{1\,1\,1\}$ and $\{2\,2\,2\}$ reflections are less than others reflections. Due to anisotropic strain, ΔK is not a linear function of K and therefore, the traditional Williamson–Hall method does not approximate ΔK well. Similar behavior was found for all Cu–Cr alloys. Fig. 3(a) shows that when using the modified Williamson–Hall method, ΔK follows smooth curves as a function of $K\bar{C}^{1/2}$, thus ΔK does not increase monotonously with the order of reflections. This phenomenon occurs in all Cu–Cr alloys studied, suggesting that the alloys contain anisotropic strain caused by dislocations. Considering that MA causes severe plastic deformation, the modified Warren–Averbach or Williamson–Hall methods give a better interpretation than traditional methods, due to anisotropic deformation produced by dislocations. The traditional Williamson–Hall method consider that strain is in the materials at random (for this reason it is used root-mean square strain $\langle\varepsilon^2\rangle^{1/2}$), and modified Williamson–Hall and Warren–Averbach methods consider that the relative atom displacement due to strain is not random. Thus, the contrast factor better represents the strain in

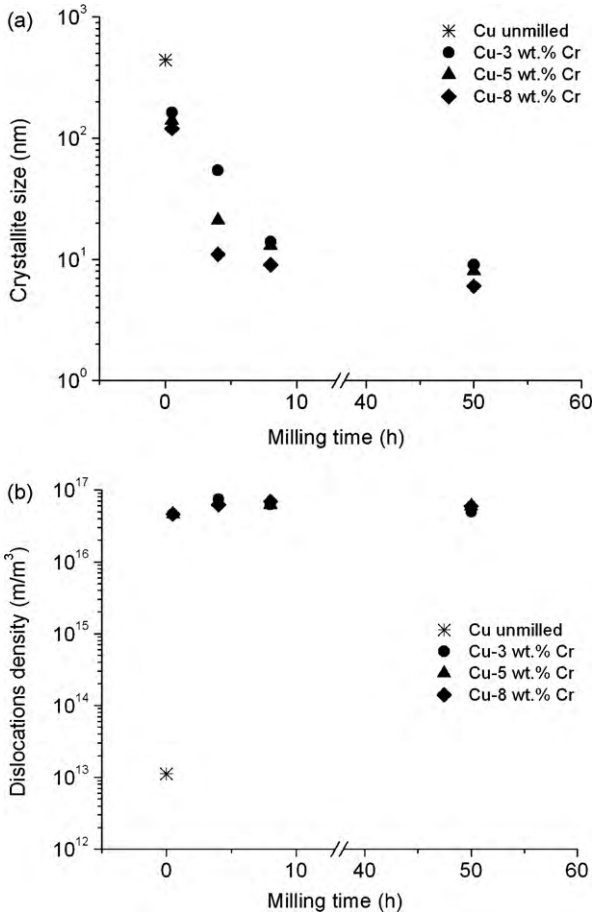

Fig. 4. The (a) crystallite size and (b) dislocation density as a function of the Cu–Cr alloy milling time.

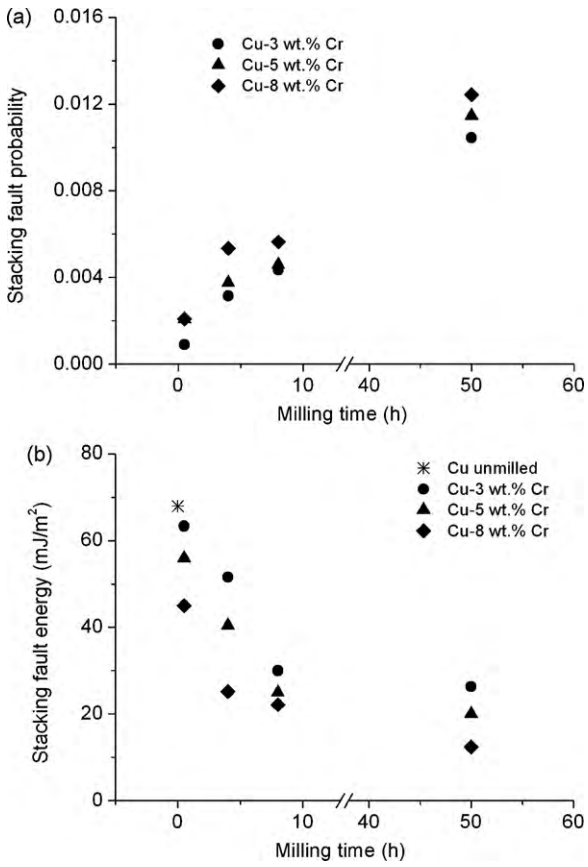

Fig. 5. Variation of (a) stacking fault probability and (b) staking fault energy as a function of Cr amount and milling time.

materials due that the correlations between displacements are long range [14].

3.1.2. Crystallites sizes and dislocation density

Fig. 4(a) shows that crystallite size (determined by modified Warren–Averbach method) decrease when milling time is increased for all Cu–Cr alloys. The crystallite size for pure Cu was around 500 and 18 nm at 0 and 50 h of milling, respectively. The crystallite size obtained after 50 h of milling is in agreement with results of Al-Hajry et al. [15], who reported a crystallite size of 14 nm for pure milled Cu. Additionally, a smaller crystallite size was obtained increasing the Cr amount, suggesting the alloy solid solution is harder and stronger than pure metal, which affects the crystallite size. The crystallite sizes are around 10 nm at 50 h, for all Cu–Cr alloys. When solute atoms are dissolved into the solid solution, they increase the hardness, increasing its fragmentation tendency [16]. This finding is in agreement with results reported by Eckert et al. [16]. Nanostructures are formed by the deformation that occurs in shear bands located in unstrained grains. The grain size (or crystalline size) decreases steadily and the shear band coalesces when milling time increases. The small angle boundaries were replaced by higher angle grain boundaries, implying grain rotation producing disclinations [17], as reflected by the absence of texture in the electron diffraction pattern and random orientation of the observed grains (contributing to X-ray peak diffraction broadening), from the lattice fringes in the high resolution electron images. Thus, dislocation free nanocrystalline grains were formed. As milling continues, the nanocrystalline grains reach a saturation value. Due to the difficulty of dislocation generation at the nanocrystalline size, the existing dislocations will rearrange and some become eliminated. For this reason, the strain and dislocation density decrease. In nanocrystalline materials, the grain size can coincide with crystallite size, due that the crystallite size is the smallest scale length in a microstructure. Fig. 4(b) shows that dislocation density (determined by modified Warren–Averbach method) increases with milling time until typical values of materials with severe plastic deformation [18,19], and then the dislocation density decreases, as mentioned above.

3.1.3. Stacking fault probability and energy

Stacking fault probability (α) was determined from peak relative shift of pair reflections {2 0 0}–{1 1 1}, {2 2 0}–{2 0 0}, and {3 1 1}–{2 2 0} [10], and stacking fault energy (γ) were calculated by Eq. (3) [20], where $K_{1\,1\,1}\omega_0$ is 6.6 ± 0.1, $G_{1\,1\,1}$ is the shear modulus in the {1 1 1} fault plane, and a is the lattice parameter.

$$\gamma = \frac{K_{1\,1\,1}\omega_0 G_{1\,1\,1} a}{\pi\sqrt{3}} \left\{ \left(\frac{b}{2\pi}\right)^2 (\pi\rho\bar{C}) \ln\left(\frac{R_e}{L}\right) \right\} \frac{1}{\alpha} \quad (3)$$

As shown in Fig. 5(a) the α values increase as milling times and Cr amounts increase. Higher α values were obtained at 50 h for all the Cu–Cr alloys, around to 10^{-2}. Similar results have been reported by other authors for copper alloys [21,22]. In early studies, α values between 10^{-2} to 10^{-3} [23,24] have been published for copper alloys. Gayle and Biancaniello [22] observed increases of α until $\approx 7.8 \times 10^{-3}$ for Cu–10%Co at 32 h of milling and Aguilar et al. [25] observed values of $\approx 8 \times 10^{-3}$ for Cu–2 wt.%Cr–6 wt.%Mo at 4 h of milling. The α increment confirms the behavior observed in Fig. 3(b), confirming the presence of anisotropic strain. Staking fault lead to less ΔK values of {1 1 1} and {2 2 2} reflections than other peaks. Finally α values are in agreement with the disloca-

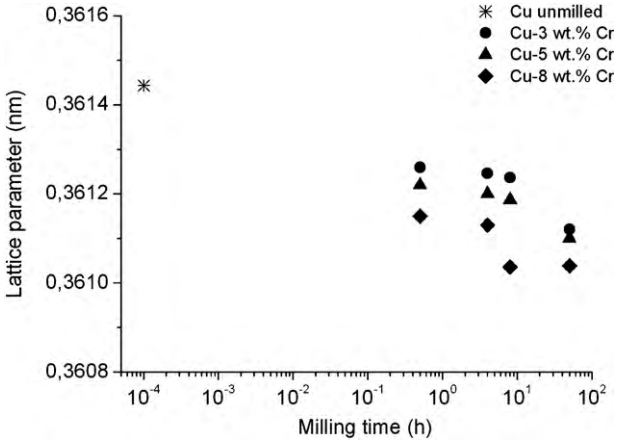

Fig. 6. Lattice parameters of the Cu–Cr alloys as a function of milling time.

tion density values [22]. When metallic powders suffer a severe plastic deformation, the dislocation density increases, as shown in Fig. 4(b). The elastic energy is proportional to Gb^2, where G is the shear modulus and b the Burger vector. Ideal and dislocation have Burger vector of $a/2[\bar{1}\,1\,0]$ and a partial dislocation of $a/6[\bar{2}\,1\,1]$. Therefore, from an energetic point of view, partial dislocation is favored, increasing the α values, which is higher in materials with low γ values, such as Cu–Cr alloys. In fcc materials, γ decreases when solute atoms enter the solvent lattice [26]. From Fig. 5(b) it is observed a decrease of γ when milling time and amount of Cr increase until values between 10 and 30 mJ/m^2. This supports the formation of a Cu–Cr solid solution.

The lattice parameter, which was calculated by Cohen's method [27], decreased when milling time and amount of Cr are increased, Fig. 6. This is because the atomic radius of Cr is lower than the atomic radius of Cu [28].

Crystallite size distributions, $\varphi(x)$, were determined by Eq. (4), assuming a log-normal distribution [29–31], where m and σ are the distribution median and variance, respectively, and d is the crystallite or grain size. The crystallite size distribution shifted to lower crystallite sizes when milling time and percentage of Cr increases, confirm a crystallite size refinement. Fig. 7 shows examples for two alloys with 5 and 8 wt.% Cr.

$$\varphi(x) = \frac{1}{(2\pi)^{1/2} d\sigma} \exp\left\{-\frac{\ln(d/m)^2}{2\sigma^2}\right\} \quad (4)$$

3.2. SEM and hardness results

All Cu–Cr alloys showed particle refinement, which was observed by SEM. Fig. 8 shows an example for of Cu-3%Cr alloy, and is a typical example of metallic powders processed by MA [3], where is shows refinement of particles. After some milling time, a thin layer is formed on the balls and inner wall of the vials [3,32]. This layer is good because it prevents contamination from the milling balls and vial wall to metallic powders. It was found that the Vickers microhardness (HV) of this layer formed on balls and microhardness of balls increased with milling time until reach 300 and 1000 HV, respectively at 50 h, as shown in Fig. 9(a) (for Cu–3%Cr alloy). Fig. 9(b) shows HV values of Cu–Cr alloys compared to pure Cu. The alloy HV values are consistently higher than the pure milled Cu HV values. The Cu–8%Cr and Cu–5%Cr alloys presents higher HV values than Cu–3%Cr for milling times of less than 8 h, but at 50 h, the HV values are similar for the three alloys. The hardness values of pure Cu milled are due to (i) strain hardening and (ii) grain boundary (or crystallite size) strengthening, and hardness values of alloys are due to the two last mechanism

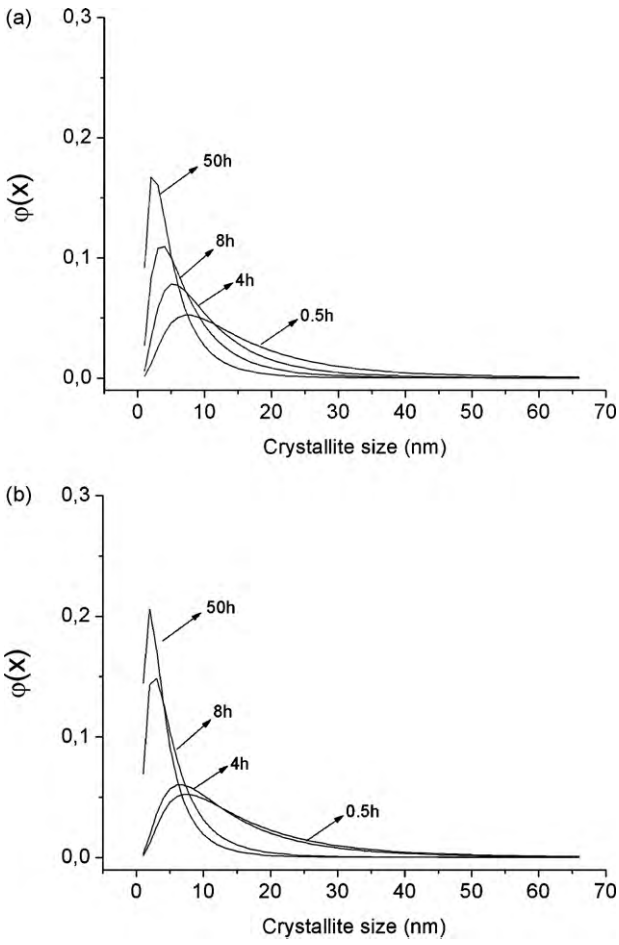

Fig. 7. Crystallite size distributions of (a) Cu–5%Cr and (b) Cu–8%Cr.

plus (iii) solid solution strengthening (assumed by disappearance of Cr diffraction lines, which occurs at high milling times, decrease stacking fault energy and lattice parameter). Finally Fig. 9(b) is in agreement with Figs. 4 and 5, due that shows that structural features changes higher of the Cu–Cr alloys produced are higher at lower milling times than 8 h.

3.3. TEM results

Fig. 10(a) shows an example of TEM image for a Cu–3%Cr alloy milled 50 h. It is possible to observe the presence of crystallites. This behavior was observed for all Cu–Cr alloys. The results shows that the crystallite size obtained from XRD, Fig. 4(a) are smaller than the crystallite size determined from TEM, this is agreement with results of another works [29,31]. The crystallites sizes calculated by X-ray methods are usually less than the ones determined by TEM micrographs [33,34], as shown the scheme of the Fig. 10(b). Size provided by XRD is the average of the smallest undistorted region in the material, whereas TEM is related to regions separated by more-or-less sharp contours in TEM micrograph. The X-ray methods can determine the size of coherently scattering domains within internal grain areas with a weakly distorted crystal lattice. Whereas the TEM method measure a complete crystallite size. The crystallite anisotropy can significantly influence the results obtained, since X-ray measures crystallite size in the direction perpendicular to the surface and TEM measures crystallite size in the plane parallel to the sample surface.

Finally can be said, the formation of solid solution is in agreement with disappearance of the strongest Cr peaks, decreases in

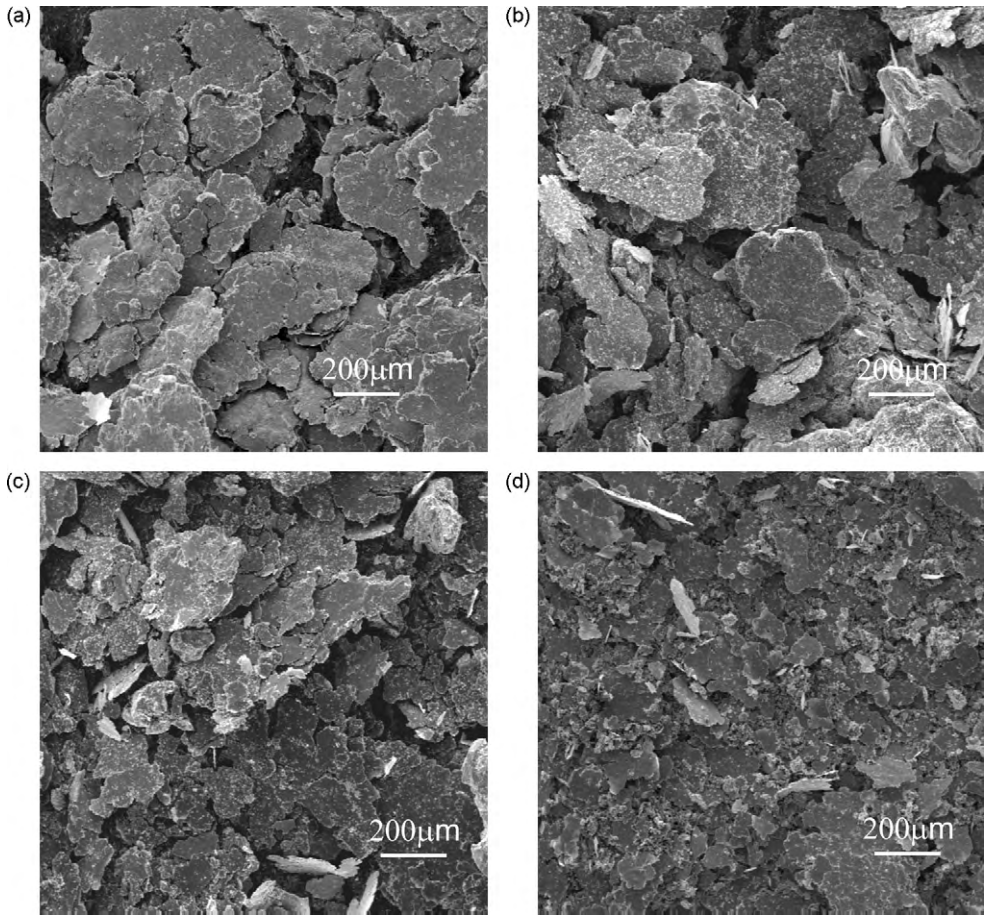

Fig. 8. SEM micrographs of Cu–3%Cr powders milled at (a) 0.5 h, (b) 4 h, (c) 8 h and (d) 50 h.

stacking fault energy, lattice parameters and crystallite sizes and distributions. Yavari [35] have proposed that the extension of a solid solution in a system with a positive mixing enthalpy can be due to presence of crystallite particles smaller than 2 nm. A fraction of the crystallites in the Cu–Cr alloys are around 2 nm, as shown in Fig. 7. Ogino et al. [36] reported similar results, for an extension of solid solution of 50%Cr in Cu. Aguilar et al. [37,38] reported that free energy stored as crystalline defects (grain boundary and elastic energy due to dislocations) at 50 h of milling is higher than the mixing free energy, ΔG^{mix} for Cu–8%Cr, as shown in Fig. 11. Fig. 12 shows a Darken–Gurry plot [3] of Cu with other metals. Between Cu and Cr, conditions exist for the formation of a solid solution, as both elements have similar atomic radius and electronegativity. The increase in crystalline defect density during milling allows for stored energy which increases the free energy of the Cu–Cr powder. Thus, free energy curves are move upwards, changing the solubility limit, and allowing a solid solution extension as has been shown by other work in mechanical alloying [39,40].

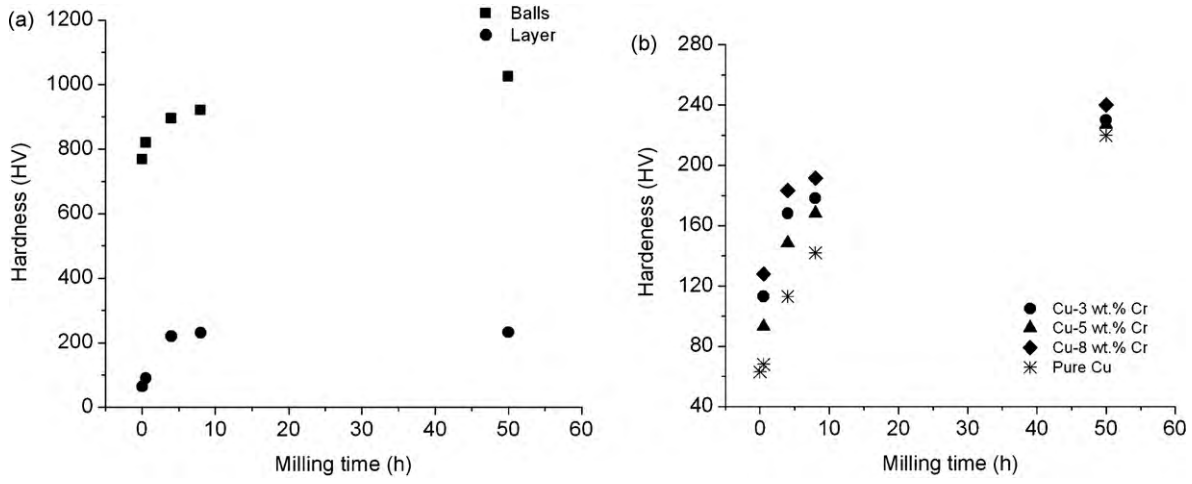

Fig. 9. Hardness Vickers of (a) layer formed on the balls and (b) Cu–Cr alloys.

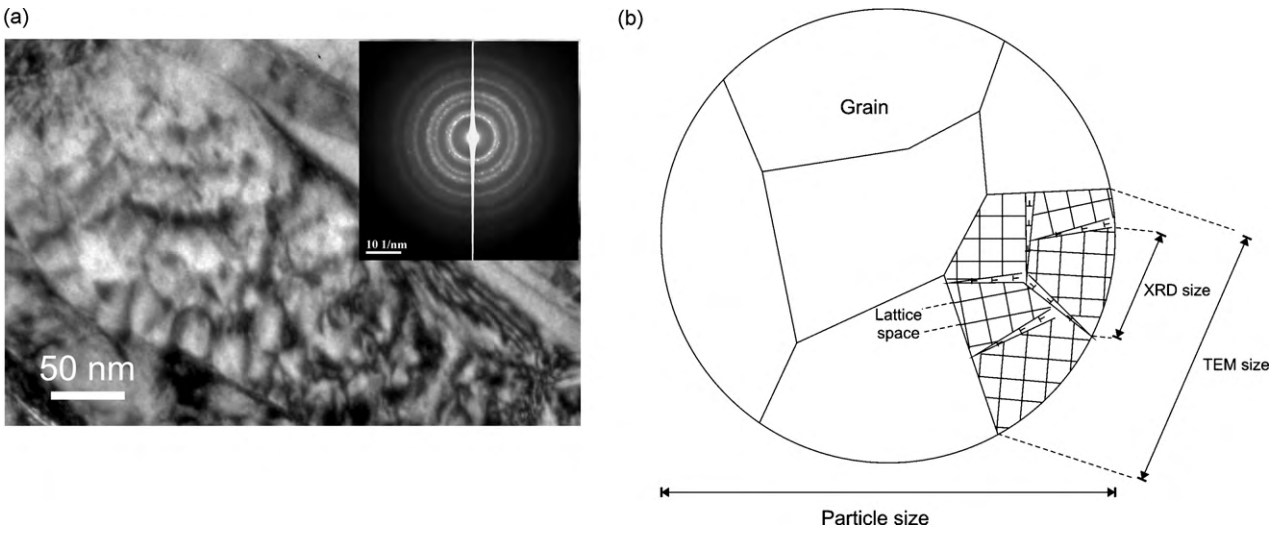

Fig. 10. (a) TEM image shows crystallite size of a Cu–3%Cr alloy at 50 h of milling and (b) schematic picture of crystallites and comparison of X-ray and TEM sizes.

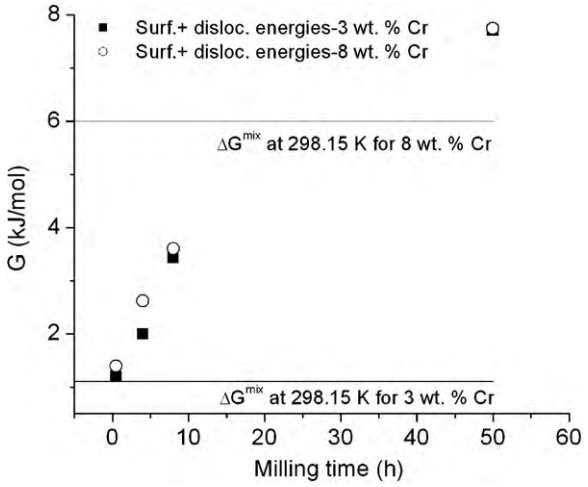

Fig. 11. Energy values, the line is the regular model assumption and the squares are the total free energy data points stored as crystalline defects for the Cu–3 and 8%Cr alloys [37].

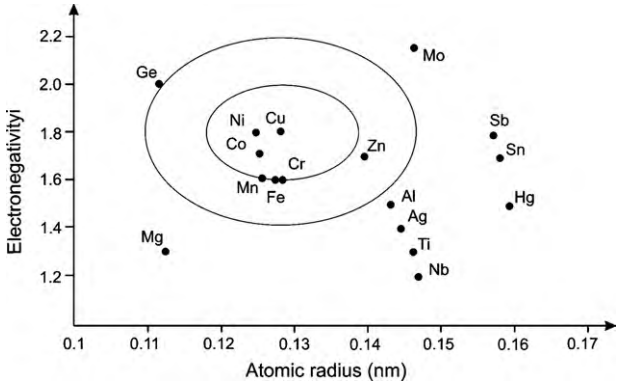

Fig. 12. Modified Darken–Gurry plot for copper [3].

4. Conclusions

The modified Williamson–Hall and Warren–Averbach methods are better interpretations of X-ray diffraction profiles than the classic methods.

Crystallite size, stacking fault energy decrease and strain, dislocation density, stacking fault probability and hardness of Cu–Cr alloys increase due to the severe plastic deformation caused by milling. Data collected in this study are in agreement with other published research in the mechanical alloying of metallic powders.

The MA process increases the crystalline defect density. Thus, the stored energy is sufficient to increase the Cu–Cr solubility. This conclusion is supported by the disappearance of the strongest Cr reflection and a reduction in the lattice parameter and stacking fault energy.

Acknowledgements

The authors would like to acknowledge support from FONDECYT-CONICYT, project No. 11070052, and Dirección de Investigación y Desarrollo de la Universidad Austral de Chile.

References

[1] C. Suryanarayana, Non-equilibrium Processing of Materials, Pergamon, 1999.
[2] T.T. Tsong, Mater. Sci. Eng. A 286 (2000) 87.
[3] C. Suryanarayana, Prog. Mater. Sci. 46 (2001) 1–184.
[4] E. Ma, Prog. Mater. Sci. 50 (2005) 413–509.
[5] Archivos PCPDFWIN, 2.4, JCPDS-ICDD, June 2003.
[6] T. Ungár, A. Borbély, Appl. Phys. Lett. 69 (1996) 3173–3175.
[7] M.A. Krivoglaz, X-ray and Neutron Diffraction in Nonideal Crystals, Springer-Verlag, 1996.
[8] M. Wilkens, Phys. Status Solidi A 104 (1987) K1–K6.
[9] T. Ungár, I. Dragomir, A. Révész, A. Borbély, J. Appl. Cryst. 32 (1999) 992–1002.
[10] B.E. Warren, X-ray Diffraction, Dover Publications, Inc., 1990.
[11] E. Tóth-Kádar, I. Bakonyi, L. Pogány, A. Cziráki, Surf. Coat. Technol. 88 (1996) 57–65.
[12] R. Hertzberg, Deformation and Fracture Mechanics of Engineering Materials, 4th ed., Jhon Wiley & Sons, 1995.
[13] G.K. Williamson, W.H. Hall, Acta Metall. 1 (1953) 22–31.
[14] T. Ungár, Scripta Mater. 51 (2004) 777–781.
[15] A. Al-Hajry, M. Al-Assiri, S. Al-Heniti, S. Enzo, J. Efne, A. Shahrani, A.E. Salami, Mater. Sci. Forum 386/388 (2002) 205–210.
[16] J. Eckert, J.C. Holzer, C.E. Krill III, W.L. Johnson, J. Mater. Res. 7 (1992) 1980–1983.
[17] A.A. Nazarov, A.E. Romanov, R.Z. Valiev, Scripta Mater. 34 (1996) 729–734.
[18] G. Ribárik, J. Gubicza, T. Ungár, Mater. Sci. Eng. A387/389 (2004) 343–347.
[19] P. Scardi, Y.H. Dong, M. Leoni, Mater. Sci. Forum 378 (2001) 132–141.
[20] S.N. Dey, P. Chatterjee, S.P. Sen Gupta, Acta Mater. 53 (2005) 4635–4642.
[21] K. Kapoor, D. Lahiri, I.S. Batra, S.V.R. Rao, T. Sanyal, Mater. Charact. 54 (2005) 131–140.
[22] F.W. Gayle, F.S. Biancanello, Nanostruct. Mater. 6 (1995) 429–432.
[23] P. Sahu, S.K. Pradhan, M. De, J. Alloys Compd. 377 (2004) 103–116.
[24] C.N.J. Wagner, J.C. Hélion, J Appl. Phys. 36 (1995) 2830–2837.
[25] C. Aguilar, V. Martínez, S. Ordóñez, O. Pavez, L. Valderrama, Rev. Met. Mad. 44 (2008) 243–250.
[26] R. Cahn, P. Haasen (Eds.), Physical Metallurgy. North-Holland, 1996.
[27] B.D. Cullity, S.R. Stock, Elements of X-ray Diffraction, 3rd ed., Addison-Wesley, 2001.

[28] W.D. Callister, Materials Science and Engineering: An Introduction, 7th ed., Wiley, 2006.
[29] C.E. Krill, R. Birringer, Philos. Mag. A 77 (3) (1998) 621–640.
[30] R.Z. Valiev, R.K. Islamgaliev, I.V. Alexandrov, Prog. Mater. Sci. 45 (2000) 103–189.
[31] T. Ungár, J. Gubicza, G. Ribárik, A. Borbély, J. Appl. Cryst. 34 (2001) 298–310.
[32] P.S. Soni, Mechanical Alloying, Cambridge International Science Publishing, 2000.
[33] N. Jia, Y.D. Wang, S.D. Wu, W.Z. Han, Y.N. Wang, J.N. Deng, P.K. Liaw, Scripta Mater. 54 (2006) 1247.
[34] Y. Zhong, D. Ping, X. Song, F. Yin, J. Alloys Compd. 476 (2009) 113.
[35] A.R. Yavari, Mater. Sci. Eng. A179/180 (1994) 20–26.
[36] Y. Ogino, S. Murayama, T. Yamasaki, J. Less Common Met. 168 (1991) 221–235.
[37] C. Aguilar, V. de, P. Martínez, J.M. Palacios, S. Ordóñez, O. Pavez, Scripta Mater. 57 (3) (2007) 213–216.
[38] C. Aguilar, V. Martínez, L. Navea, O. Pavez, M. Santander, J. Alloys Compd. 471 (2009) 336–340.
[39] S. Xi, K. Zuo, X. Li, G. Ran, J. Zhou, Acta Mater. 56 (2008) 6050–6060.
[40] J.S. Blzquez, J.J. Ipus, M. Millán, V. Franco, A. Conde, D. Oleszak, T. Kulik, J. Alloys Compd. 469 (2009) 169–178.